Theoretical interpretation of scanning tunneling microscopy images: Application to the molybdenum disulfide family of transition metal dichalcogenides

Terry R. Coley, William A. Goddard III, and John D. Baldeschwieler
Contribution No. 8184 from the Arthur Amos Noyes Laboratory of Chemical Physics, California Institute of Technology, Pasadena, California 91125

(Received 24 July 1990; accepted 7 November 1990)

We have performed *ab initio* quantum mechanical calculations to describe scanning tunneling microscopy (STM) images of MoS_2 and $MoTe_2$. These results indicate that the interpretation of the STM images of these and related materials depends sensitively on experimental conditions. For example, determining whether the maximum tunneling current correlates to the top atom (S or Te) or to the second-layer atom (Mo) requires information on the tip-sample separation. Based on these results we discuss some STM experimental procedures which would allow assignment of the chemical identity of STM spots with greater certainty.

I. INTRODUCTION

Scanning tunneling microscopy (STM) has clearly demonstrated its usefulness as a real-space atomic resolution surface probe. A striking example is the overwhelmingly conclusive evidence STM has provided for the correctness of the Takayanagi model[1] for the 7×7 reconstruction of the Si(111) surface.[2] In contrast to these successes, however, there remain many examples of STM images leading to ambiguous answers about the surface system in question. For example, many groups have imaged the transition metal dichalcogenides,[3–6] but have disagreed in the interpretation of these images. The difficulty arises from the fact that the sample is heteroatomic, but the different elements reside in symmetry equivalent positions when projected onto a viewing plane parallel to the surface (see Fig. 1, top). Interpreting these images, therefore, requires a quantitative understanding of the electronic structure of the tip-sample system and the mechanism for electron transfer. As we will show, correct chemical assignment of the STM peaks in images of the MoS_2 family of compounds is one case where a detailed theoretical study is necessary to resolve ambiguities which arise due to the inherent symmetry of the system.

Because of their interesting electronic and mechanical properties,[7,8] the transition metal dichalcogenides have been the subject of numerous theoretical and experimental studies. Many of these properties arise from the layered structure of these materials. In particular, 2H – MoS_2, 2H – $MoSe_2$, and 2H–$MoTe_2$ consist of X–Mo–X (X = S,Se,Te) trilayers each with a central layer composed of hexagonally arranged Mo atoms. Each Mo has trigonal prismatic coordination to six X. See Fig. 1. The lack of covalent bonds between X–Mo–X sandwiches is a primary factor leading to the lubricative properties of MoS_2. This also allows easy cleavage to expose large areas of atomically flat MoX_2. These surfaces are sufficiently inert to be imaged by STM in air.[6]

Detailed information about the electronic structure of these surfaces is a prerequisite to predicting any useful materials modifications for attaching these compounds to substrates while retaining efficient lubricative properties. For this reason STM and scanning tunneling spectroscopy (STS) studies of the MoS_2 family of materials have been undertaken by many groups. However, attempts to interpret the results have been complicated by the high degree of symmetry present in the images: high quality fast-scan images (constant height) show three equivalent hexagonal lattices of high, medium, and low current.[5] The assignment of Mo, X, and crystal hollow to each of these current levels is there-

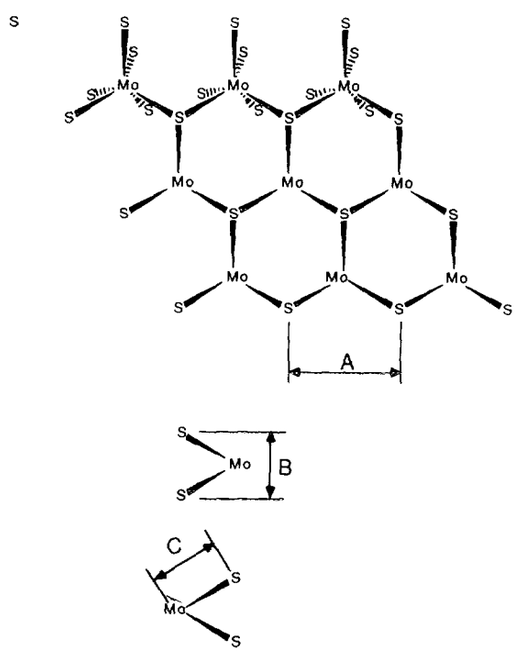

FIG. 1. Structure of the MoS_2 family of layered transition metal dichalcogenides (S = S or Te). Top: looking down on surface; first row of Mo indicates the trigonal prismatic coordination to the lower layer of chalcogenide. Bottom: cross section showing stacking of sandwich layers. Dimensions[21] for MoS_2: A = 3.16 Å, B = 2.98 Å, C = 2.41 Å. Dimensions[22] for $MoTe_2$: A = 3.52 Å, B = 3.63 Å, C = 2.72 Å.

 0734-211X/91/020470-05$01.00

fore ambiguous without some assumptions about the electronic structure of the surface. Various authors have presented differing interpretations of these images with the concomitant differing arguments to justify them.[3–6] In summary, proximity to the tip argues for dominance of the chalcogenides, while the Mo d_{z^2} character of the states near the Fermi level argues for the metal's dominance.

Tang, Kasowski, and Parkinson[6] have in particular made progress experimentally with regard to correct assignment of the STM peaks. They have imaged WTe_2 which contains staggered (and therefore symmetry inequivalent) W atoms in the second plane. These images clearly showed dominance of the metal in the images. However, it was not clear if these results could be used unambiguously to predict that the peaks in their images of $MoTe_2$ were also due to the metal: uncertainty arises because W is octahedrally coordinated to Te while Mo is trigonal-prismatically coordinated. Furthermore, they performed an approximate calculation to determine the density of states above the surface. Their results indicated the spatial distribution of the density of states near the Fermi energy to be greatest over the Te atoms, which in the Tersoff and Hamann formalism[9] would indicate a greater tunneling current over the Te. Clearly, ambiguity still exists in the correct assignment of images in the MoS_2 family of materials. A major goal of this theoretical investigation is to provide firm ground for making interpretations of these images.

II. THEORETICAL MODEL

A. Tip-sample model

Models were developed specifically to describe the electronic structure of MoS_2 and $MoTe_2$ in the presence of a tip. Hartree–Fock wave functions for the tip-sample system were computed for various positions of the tip above the sample. For each geometry two predominant electronic states were studied: the first state described a hole (acceptor orbital) on the tip; the final state had the hole in the sample (one electron was transferred to the tip). For each tip-sample geometry, an all-valence-electron resonance calculation between the two states was performed.[10] The resulting transfer matrix element describes the amount of coupling between the two many-electron quantum states. Differences in the transfer probability as a function of tip position reflect the overall changes in tunneling current expected from a true tip-sample system with bulk orbitals composed of a linear combination of the cluster states as a basis.

B. Model for the MoX_2 bulk

The particular clusters used for MoS_2 and $MoTe_2$ consist of seven Mo atoms arranged in a centered hexagon with the six chalcogenide atoms arranged in a trigonal prism. Figure 2 shows the geometry of this cluster. For the central Mo we used Hay and Wadt's[11] valence double-zeta basis set and effective core potential (ECP). This basis was contracted to a minimum basis set for the six external Mo atoms. The chalcogenides were also treated at the valence double-zeta level. The Hay and Wadt basis and ECP were used for Te, and the Rappe, *et al.*[12] basis and ECP were used for S.

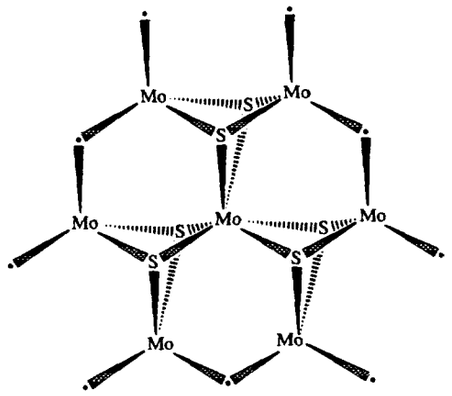

FIG. 2. Structure of the cluster to model MoS_2 and $MoTe_2$ (S = S or Te). The positions of all atoms are taken from the bulk structure (see Fig. 1). Dots represent point charges which replace the chalcogenide nuclei at the other end of the dangling bonds. Only nine point charges are shown; nine more exist in the second chalcogenide plane.

Much attention was paid to designing this cluster to mimic the bulk system. The cluster gives the proper chemical bonding environment to the central MoX_6 trigonal prism: all bonds are satisfied as in the bulk. The treatment of the exterior Mo atoms was constructed so that the Mo *d* electrons were distributed in as many orbitals as would exist if the exterior Mo atoms were fully contained in the bulk. Each Mo has six valence electrons, two of which end up in a nonbonding d_{z^2} orbital. The other four can be thought of as contributing equally to six Mo–X bonds, 2/3 electron to each bond. Therefore, since each Mo of the exterior ring has four broken bonds and a d_{z^2} orbital, 28 electrons should occupy the 30 orbitals representing the dangling bonds and nonbonding orbitals at the cluster edge. However, we require an integral number of electrons per orbital (we cannot use an effective Hamiltonian) in the cluster for calculation of many-electron matrix elements. Thus, we added two electrons resulting in an overall charge of -2. The electrons in these orbitals were coupled high spin to prevent back bonding to the center of the cluster. The charge of the cluster was also made neutral by adding 18 counter charges of $+0.11e$ placed at the positions of the chalcogenide nuclei that the exterior Mo atoms would be bonded to. This further served to direct the exterior *d* electrons toward the missing centers they would normally be bonded to. The result of this work is a chemically well described core trigonal prism of material.

C. Quality tests for the bulk model

We found Mo_7X_6 to be the minimum cluster necessary to give a good description of the surface. Attempts to use a naked trigonal prism (MoS_6) without the surrounding ring of Mo resulted in an ordering of molecular orbital (MO) states which did not reflect the bulk band structure.[13] This was the result of inadequate lowering of the chalcogenide *p*-orbital energies when the full bonding environment to Mo was not established. Results with MoS_6 clusters gave ionization potentials for the surface of 7–8 eV while a neutral

Mo_7S_6 cluster gives 5.2 eV, much closer to the experimental bulk work function of 4.90 ± 0.15 eV.[7]

Because the basis set consists of Gaussian functions, we were careful to ensure that the resulting wave functions behaved with proper exponential decay in the region between tip and sample. Figure 3 shows a log plot of the wave function amplitude for the highest energy occupied MO (HOMO) of the tip-sample system which is primarily Mo d_{z^2} in character. The plot shows the expected exponential decay in the vacuum region.

As an additional test of the quality of our wave function, we augmented the basis set on the S directly below the tip atom in the Mo_7S_6 cluster to contain two additional diffuse functions.[14] The most diffuse of these functions had a radial exponent which provided a slower falloff into the vacuum than the Mo functions. Even with diffuse functions on the sulfur, the quantitative results were modified by 20% at most and the qualitative conclusions we will draw remain the same.

In summary, we have shown that Mo_7X_6 is a carefully crafted, successful model for the MoX_2 bulk. It has the advantage of being a wholely self-consistent all-valence electron description of a chemically relevant section of the crystal.

D. The tip

The STM system also contains a tip modeled by a Ba atom. Ba was chosen because its ionization potential of 5.2 eV closely matches the bulk work function for tungsten. W is used as the tip material for many STM experiments, including those on MoX_2. In our model the s orbital of the Ba atom will serve as the accepting orbital present at the end of the STM tip.

E. Tunneling current

As mentioned earlier, two states are calculated: Ψ_A is the self-consistent N-electron wave function having a hole (acceptor) on the tip while Ψ_B is the self-consistent wave function having a hole in the sample. The matrix element describing the tunneling probability for a two state system is

$$T_{BA} = (H_{BA} - S_{AB}H_{AA})/(1 - |S_{AB}|^2) ,$$

where

$$H_{BA} = \langle \Psi_B | H | \Psi_A \rangle$$

$$H_{AA} = \langle \Psi_A | H | \Psi_A \rangle$$

$$S_{AB} = \langle \Psi_A | \Psi_B \rangle ,$$

and H is the full N-electron Hamiltonian. Since Ψ_A and Ψ_B are the fully relaxed many-electron wave functions, these calculations include the response of the other N-1 electrons to the electron transfer process.

The use of T_{BA} to describe electron transfer rates is well established in the chemical literature.[15,16] Its relationship to solid-state electron transfer theory is clearly described in West *et al.*[17] and is derived from Bardeen's time-dependent, first-order perturbation theory.[18] It is important to note that for each matrix element above, the full valence electron Hamiltonian of the system is evaluated with respect to the determinantal wave functions Ψ_A and Ψ_B. Ultimately, the matrix element calculations reduce to evaluating integrals where the integrand contains Gaussian functions (from the basis set expansion of the wave function) centered at various atomic positions and operated on by the one and two electron terms in the Hamiltonian. Such calculations are ubiquitous in modern molecular quantum chemistry,[19] however, evaluation of the cross matrix element H_{AB} between two nonorthogonal, N-electron, determinantal wave functions requires a prior biorthogonalization procedure in order to avoid $N!$ expansion of the time for evaluation of these matrix elements.[10]

The theory above is derived in the small bias voltage limit. In fact, the above formalism describes electron transfer between just two states of the tip and sample. In practice, as the bias voltage is increased many more states are sampled for electron transfer. We consider one band of states, the valence d_{z^2} band. To calculate the total experimental tunneling current, it would be necessary to sum the contributions from all states in the d_{z^2} band derived from our single lattice site basis. We do not do that here, but rather focus on the intuition gained from studying the underlying coupling constants between states of the tip and sample in a localized region above the surface. An additional effect of the bias voltage is that a strong field is generated between the tip and sample. If the surface state is sufficiently polarizable, this could modify the shape of the surface wave function enough to change the qualitative peaks in the tunneling current as a function of position. We tested this case by generating a new set of tip-sample system wave functions converged under a field corresponding to tip-positive by 1 V. Although, the relative energies of states in the bulk change slightly, there was no effect on the relative current as a function of tip position from that predicted by the matrix elements at close to zero field which we present here.

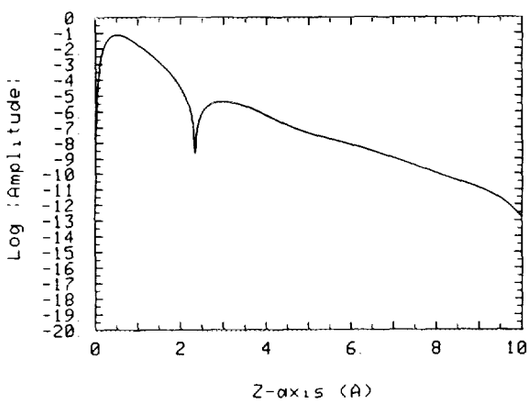

FIG. 3. Log plot of the absolute amplitude of the HOMO (donor orbital) in the $MoS_2 \cdots$ Ba sample-tip system. The amplitude is calculated along a line perpendicular to the surface and passing through the central Mo and the Ba. The Mo plane is at $z = 0$ Å, the S plane is at $z = 1.49$ Å, and the Ba tip is at $z = 10.0$ Å.

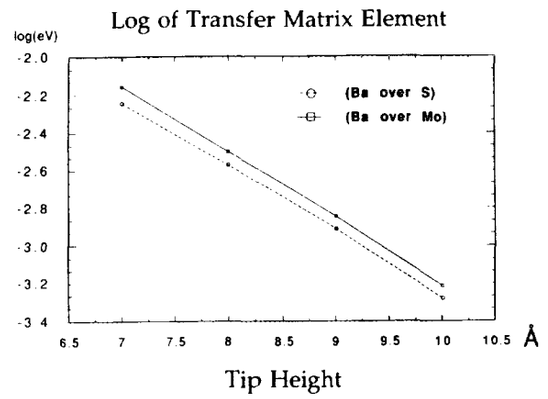

FIG. 4. Log plot of T_{BA} for the $MoS_2 \cdots$ Ba sample-tip system as a function of tip atom distance over the Mo plane (at 0 Å). For the solid line, the tip was over the central cluster Mo. For the dashed lined, the tip was over a cluster *S*. The units of T_{BA} were eV.

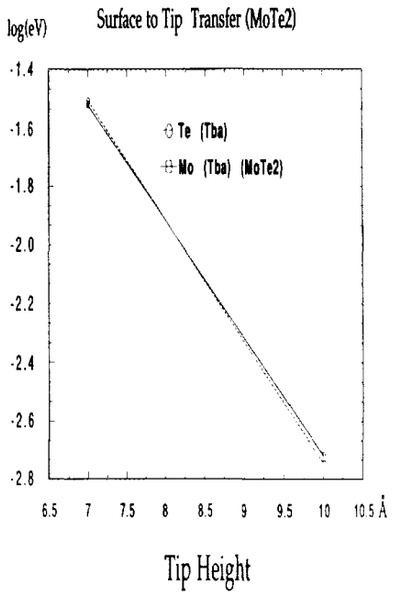

FIG. 5. Log plot of T_{BA} for the $MoTe_2 \cdots$ Ba sample-tip system as a function of tip atom distance over the Mo plane (at 0 Å). For the solid line, the tip was over the central cluster Mo. For the dashed lined, the tip was over a cluster Te. The units of T_{BA} were eV.

III. RESULTS SUMMARY

A. MoS_2

Figure 4 shows a log plot of the transfer matrix element T_{BA} at four tip-sample separations and at two lateral positions above the surface. The solid line shows the behavior of T_{BA} while the tip atom is over the central Mo, the dashed shows T_{BA} with the tip directly above a sulfur. We see that the electronic coupling T_{BA} is larger with tip over the Mo for all tip-sample separations explored. We also see an exponential decay of T_{BA} as expected from the exponential decay of the wave function.

B. $MoTe_2$

Figure 5 shows a plot for $MoTe_2$ similar to that for MoS_2. Unlike the MoS_2 plot no clear trend of dominance appears for electronic coupling over the Mo versus the Te. The calculations suggest that the coupling magnitude *may* cross at some tip-sample separation.

IV. DISCUSSION

A. Comparison of MoS_2 and $MoTe_2$

Comparison of MoS_2 and $MoTe_2$ shows an overall greater coupling between $MoTe_2$ and the tip at corresponding tip heights. This is to be expected from the more diffuse Te *p* orbitals and lower ionization potential. Thus, for the same current set point we expect the tip to glide higher over $MoTe_2$ than MoS_2.

B. Predictions for $MoSe_2$

Based on the trends for MoS_2 and $MoTe_2$ we expect $MoSe_2$ to couple with some intermediate strength to a tip. As in MoS_2, coupling will dominate while the tip is over Mo. This is based on the clear Mo dominance in MoS_2 and the nearly flat contrast seen for $MoTe_2$.

C. Experimental consequences

Our results suggest that based on electronic effects alone, there is good reason to believe that it is the second-layer Mo sites which give rise to the largest current in tip-positive STM images of MoS_2. Our results predict this trend will persist for even closer tip-sample distances, than those calculated. However, at very close distances the form of the surface wave function suggests a reversal of the image-dominant atom from Mo to S will occur. This is due to the presence of roughly 27% sulfur *p* character in the HOMO. At present, we do not know if this will occur before breakdown of gap resistance. As described next, we have proposed an experiment to resolve these tip-height issues.

The theoretical results for $MoTe_2$ show the electronic surface in the region from 5.5 to 8.5 Å above the Te is quite planar; thus, little corrugation is expected from variations in tunneling probability. One possible explanation for the corrugation observed by Tang, Kasowski, and Parkinson[6] might involve a mechanism like that proposed by Zheng and Tsong[20] for atomic resolution images of metal surfaces. This mechanism relies on the presence of an impurity on the tip with appropriate energy states to allow a resonance tunneling effect which is then modulated by the changing position of the impurity due to its response to the forces it experiences while trapped between the tip and sample. A simpler explanation for the $MoTe_2$ system brought to light by our calculations is that the tip is *closer* than 5.5 Å from the surface so that the electronic differences between Mo and Te and their differing distances from the tip are exaggerated. Since the primary character of the states near the Fermi level is Mo d_{z^2}, the tip could approach much closer to the Te surface without establishing a conductive contact (loss of gap resistance). In this case the Te layer simply serves to modulate the underlying donor states in the Mo d_{z^2} band. We plan to explore closer distances with further detailed calculations.

Based on our results for $MoTe_2$ we have also devised a new STM experiment in collaboration with Youngquist, Driscoll, and Baldeschwieler which should help distinguish between possible imaging mechanisms and provide information needed to make a definite chemical assignment. The experiment is designed to collect images at multiple tip heights free of lateral drift. We hope to show experimental evidence for the possible crossover of Mo versus Te dominance in images taken at different heights. Establishing the existence or absence of this crossover is very important to correct interpretations of these images: if the chemical assignment is tip-height dependent, careful probing of in-phase images at multiple heights will become a prerequisite to the correct chemical assignment of peaks in STM images of these and other materials.

V. ACKNOWLEDGMENTS

This research was supported in part by a grant (No. AFOSR-88-0051) from the Air Force Office of Scientific Research and the Office of Naval Research (N00014-86-K-0214). Preliminary studies were carried out earlier with funding from Hughes Aircraft Company (Mike Gardos). Additional funding came from the National Institutes of Health (R01 GM 37226-03). Calculations were performed on Alliant FX/8-8 and FPS Computing Model 511 minisupercomputers.

[1]K. Takayanagi, Y. Tanishiro, M. Takahashi, and S. Takahashi, J. Vac. Sci. Technol. A **3**, 1502 (1985).
[2]G. Binnig, H. Rohrer, Ch. Gerber, and E. Weibel, Phys. Rev. Lett. **50**, 120 (1983).
[3]H. Bando, H. Tokumoto, W. Mizutani, K. Watanabe, M. Okano, M Ono, H. Murakami, S. Okayama, Y. Ono, S. Wakiyama, F. Sakai, K. Endo, and K. Kajimura, Jpn. J. Appl. Phys. **26**, L41 (1987).
[4]G. Stupian and M. Leung, Appl. Phys. Lett. **51**, 1560 (1987).
[5]M. Weimer, J. Kramar, C Bai, and J. D Baldeschwieler, Phys. Rev. B **37**, 4292 (1988).
[6]S. L. Tang, R. V. Kasowski, and B. A. Parkinson, Phys. Rev. B **39**, 9987 (1989).
[7]J. C. McMenamin and W. E. Spicer, Phys. Rev. B **16**, 5474 (1977).
[8]P. D. Fleischauer, Thin Solid Films **154**, 309 (1987).
[9]J. Tersoff, and D. R. Hamann, Phys. Rev. Lett. **50**, 1998 (1983).
[10]A. F. Voter, Ph.D. thesis, California Institute of Technology, Pasadena, 1983. (Further improvements by J-M. Langlois).
[11]P. J. Hay and W. R. Wadt, J. Chem. Phys. **82**, 270 (1985).
[12]A. K. Rappe, T. A. Smedley, and W. A. Goddard III, J. Phys. Chem. **85**, 1662 (1981).
[13]R. Coehoorn, C. Haas, and R. A. de Groot, Phys. Rev. B **35**, 6203 (1987).
[14]Two additional *s* and two additional *p* exponents were scaled out from those of Ref. 12. *s* function: 0.0499, 0.0164; *p* function: 0.0435, 0.0125.
[15]N. R. Kestner, J. Logan, and J. Jortner, J. Phys. Chem. **78**, 2148 (1974).
[16]J. Logan, and M. D. Newton, J. Chem. Phys. **78**, 4086 (1983).
[17]P. West, J. Kramar, D. V. Baxter, R. J. Cave, and J. D. Baldeschwieler, IBM J. Res. Develop. **30**, 484 (1986).
[18]J. Bardeen, Phys. Rev. Lett. **6**, 57 (1961).
[19]A. Szabo and N. S. Ostlund, *Modern Quantum Chemistry: Introduction to Advanced Electronic Structure Theory*, 1st ed. (Macmillan, New York, 1982).
[20]N. J. Zheng, and I. S. T. Tsong, Phys. Rev. B **41**, 2671 (1980).
[21]R. W. G. Wyckoff, *Crystal Structures*, 2nd ed. (Wiley, New York, 1963), Vol. 1, p. 280.
[22]D. Puotinen and R. E. Newnham, Acta. Crystallogr. **14**, 691 (1961).